IEEE Access
Multidisciplinary | Rapid Review | Open Access Journal

Received 14 September 2022, accepted 1 October 2022, date of publication 10 October 2022, date of current version 13 October 2022.

*Digital Object Identifier 10.1109/ACCESS.2022.3213067*

RESEARCH ARTICLE

# Design and Optimization of Compact Microstrip Wideband Bandpass Filter Using Taguchi's Method

**WEI-CHUNG WENG, (Senior Member, IEEE)**
Department of Electrical Engineering, National Chi Nan University, Puli, Nantou 54561, Taiwan
e-mail: wcweng@ncnu.edu.tw

This work was supported in part by the Ministry of Science and Technology of Taiwan, R.O.C. under Grant MOST 110-2221-E-260-007.

**ABSTRACT** This study presents a global optimization technique, Taguchi's method, in conjunction with a full-wave electromagnetic simulator, to optimize a novel microstrip bandpass filter operating at 2.45 GHz to achieve wideband and high selectivity characteristics. The proposed wideband bandpass filter consists of multiple parallel edge-coupled lines, which offer inherent transmission zeros to improve the selectivity. The proposed bandpass filter is fabricated on a Rogers RO 4003C substrate with a compact size of 0.25 $\lambda$g by 0.28 $\lambda$g. Sufficient information, such as the filter design procedure and the optimization settings for Taguchi's method, is described in this paper. After Taguchi's optimization, the measured results of the proposed filter show superior outcomes. A 3 dB fractional wide bandwidth of 55.2%, a minimum insertion loss of 0.43 dB, and a return loss of more than 15 dB within the passband are achieved. Furthermore, high selectivity and steep skirt within the stopbands are also obtained. In addition, the simulated and measured scattering parameters agree well with each other, which demonstrate the validity of the proposed design.

**INDEX TERMS** Bandpass filter, microstrip, optimization, Taguchi's method, wideband.

## I. INTRODUCTION

Bandpass filters (BPFs) are widely used in communication systems. A compact microstrip BPF needs to have wideband characteristics and low variations of group delay in the passband. In addition, the characteristics of high attenuation and steep skirt in the stopband are also demanded. Conventional circuit models using lumped components can be applied to design and analyze a BPF. The approximate equivalence between the microstrip BPF and the lumped-component BPF can be established using Richards' transformation and Kuroda's identity [1]. However, results obtained by this approach are usually inaccurate and not agreeing well with those obtained by full-wave electromagnetic (EM) simulators or measurements since effects of discontinuity and couplings between lines are not considered. Instead, a full-wave EM simulator can be employed to provide accuracy results to design microstrip BPFs since it predicts EM behavior well.

Conventional Taguchi's method [2] has been developed based on the concept of statistics and orthogonal array (OA), which ensures a balanced and fair selection of parameters in all possible combinations and can effectively reduce the number of tests required in a design process. However, the optimization performance of conventional Taguchi's method is limited due to the lack of an iterative process. In 2007, an iterative version of Taguchi's method was proposed [3], [4] and it demonstrated significantly better optimization performance than particle swarm optimization (PSO) method on the antenna array factor optimization. In [3], a 20-element linear antenna array was optimized to realize a sector beam radiation pattern using the iterative Taguchi's method; 70% reduction in the calculation was reported compared with the PSO method for the same antenna array. Therefore, the iterative version of Taguchi's method (denoted as the Taguchi's

The associate editor coordinating the review of this manuscript and approving it for publication was Wei Liu.

method in this study) can be considered as a global optimization technique. The Taguchi's method has been demonstrated excellent optimization capabilities in simple implementation, well handling discontinuous and nondifferentiable problems, effective reduction of test trials, fast convergence speed, global optimum results, and independence from initial values of optimization parameters [4] and it has been adopted in many electromagnetic applications since then. In the field of antenna design, the Taguchi's method has been applied to successfully achieve the designs of UWB antenna [4], slot antenna [5], and dual band T-slotted patch antenna [6]. Also, the Taguchi's method has optimized the array factor of an 80-element aperiodic planar array to obtain low side lobe levels [7]. Furthermore, in other fields, the Taguchi's method can also be employed to optimize radio network parameters for the vertical sectorization deployment [8] and for long term evolution system [9], as well as to find the optimum values of the model parameters for a Jiles-Atherton hysteresis model [10].

Nevertheless, in the field of microwave filter design, to date, few microstrip BPFs have been designed and optimized using the Taguchi's method. Hence, in this study, the in-house developed Taguchi's method is adopted and in conjunction with a method of moments (MoM) based full-wave EM simulator, IE3D [11] to optimize a novel microstrip wideband BPF operating in the WLAN 2.4 GHz band. The aim of this design is to achieve the BPF having characteristics of wide bandwidth, low insertion loss (IL) and high return loss (RL) within the passband. In addition, high selectivity and steep skirt within the stopbands are required. The Taguchi's method, which is performed using MATLAB R2020b version, is employed as an external optimizer to drive IE3D. After establishing the optimization goals, the optimization process is completely processed by the Taguchi's method to automatically search for the optimal results. This innovative and fully automatic design technique makes the design results performing high quality and effectiveness. After the Taguchi's optimization, the proposed wideband BPF is obtained. The proposed wideband BPF highly satisfies the design specifications with a compact size. Simulated and measured results of the proposed wideband BPF are also found in good agreement with each other, showing the validity and accuracy of the design using the proposed method.

The novelty of this paper is the sufficient information such as guidelines for optimization range of a parameter and proper settings for fitness function. This allows the Taguchi's method to optimize the wideband bandpass filter rapidly and successfully.

## II. WIDEBAND BANDPASS FILTER MECHANISM AND DESIGN

### A. THE MECHANISM OF THE WIDEBAND BPF

A conventional two-stage parallel coupled line shown in Fig.1 (a) can be modified by mirroring the output feeding line and folding the middle transmission line into a U-shaped, open-

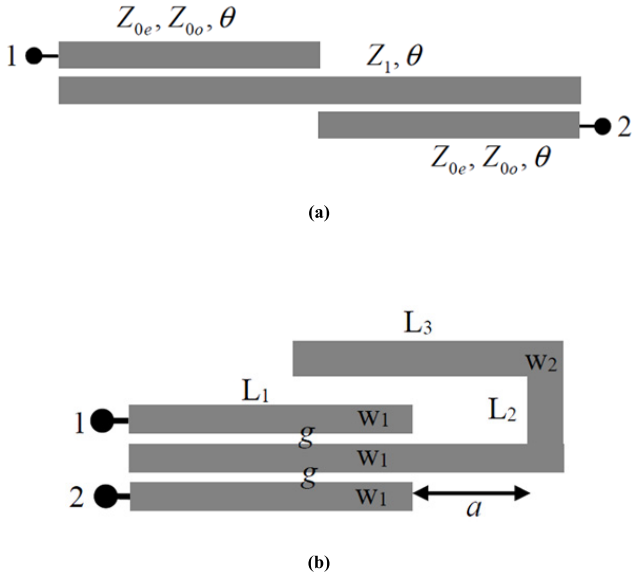


**FIGURE 1. Schematics of two-stage parallel-coupled lines. (a) Conventional two-stage, parallel-coupled lines and (b) modified two-stage, parallel-coupled lines.**

circuited line to form a BPF [12] as shown in Fig. 1(b). The two modified open-circuited stubs with the same width of $w_1$ and length of $L_1$ are parallel edge-coupled to a U-shaped, open-circuited line. The length of the two modified open-circuited stubs ($L_1$) is approximately a quarter guided wavelength ($\lambda g$) and $L_1$ can offer inherent transmission zeros (TZs) in every frequency range of [ $2n\ f_0$, $2(n+1)\ f_0$ ] [13], where the center frequency ($f_0$) is designed at 2.45 GHz and $n$ is an integer. Meanwhile, it is desired that the transmission zeros are located near the passband to improve the selectivity of the BPF. The transmission zeros can also be controlled by adjusting the width ($w_2$) and the length (the sum of $a$, $L_2$, and $L_3$) of the U-shaped, open-circuited line. Furthermore, a spacing of $g$, between the three intercoupled lines, determines the coupling effects. The smaller the $g$ is, the stronger the coupling effects obtain. Moreover, a stronger coupling strength will create a wider 3 dB fractional bandwidth (FBW), and vice versa [12]. Therefore, for a wideband BPF design, $g$ should be as small as possible. In this BPF design, $g$ is fixed at 0.12 mm, which is restricted to the precision of the manufacturing using printed circuit board (PCB) technology. Eventually, two sections of the modified parallel side-coupled lines are symmetrically connected by a strip with the width of $w_1$ and the length of $(2L_4+w_1)$ to form the proposed wideband BPF. The layout of the BPF is illustrated in Fig. 2, which is horizontally symmetric.

In Fig. 2, an open-circuited line with a length of $L_5$ and width of $w_1$ connected between two sections is utilized to suppress the second harmonic around 5 GHz ($2f_0$). The 50 Ω feeding line has a corresponding width of $w_{50}$ and a length of $L_{50}$, for the input and output ports. A tapped line having the length of $L_6$ and widths of $w_3$ and $w_{50}$ at the two ends,

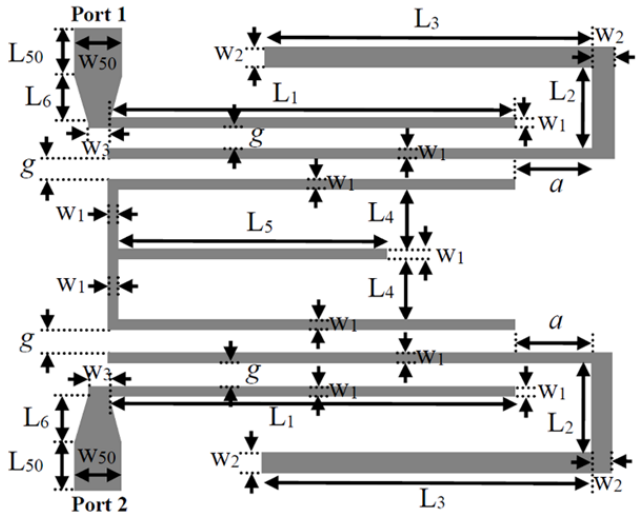


**FIGURE 2.** Layout of the proposed wideband BPF.

respectively, is used to connect the 50 Ω feeding line and the open-circuited line. By adjusting the length of $L_6$, a good impedance match can be obtained in the passband.

### B. DESIGN SPECIFICATIONS

The design specifications of the proposed wideband BPF are that the BPF will operate at 2.45 GHz, which is the center frequency of WLAN band. The BPF should have a 3 dB FBW larger than 50%, a passband $|S_{11}|$ less than −15 dB, and a stopband $|S_{21}|$ less than −30 dB. Moreover, the proposed BPF is to be fabricated on a *Rogers* RO 4003C substrate with a thickness ($h$) of 0.813 mm, a relative dielectric constant ($\varepsilon_r$) of 3.55, and a loss tangent of 0.0021.

## III. TAGUCHI's METHOD AND BPF OPTIMIZATION

### A. CONCEPTS OF TAGUCHI's METHOD

Fig. 3 shows the flow diagram of the Taguchi's method in conjunction with a full-wave electromagnetic simulator for optimizing the proposed wideband BPF. The Taguchi's optimization procedure starts with problem initialization, which includes setting optimization parameters, selecting a suitable OA, designing the initial BPF in an EM simulator, and defining the optimization goal and fitness function. Table 1 shows an orthogonal array, OA(18, 7, 3, 2) [14], which can offer 18 rows ($n = 1$ to 18) for 18 experiments (i.e. EM simulations in this study) and seven columns ($k = 1$ to 7) for seven optimization parameters with three-level ($s = 1$ to 3) entries and two strengths, is to be adopted in the optimization. The entry of the OA($n$, $k$) is $s = 1, 2,$ or 3 which represents the level values $x_k|_t^1$, $x_k|_t^2$, and $x_k|_t^3$, respectively. Where, $k$ indicates the $k$-th optimization parameter; the subscript indicates the current ($t$-th) iteration; the superscript indicates the level 1, 2, or 3. For the $n$-th experiment in the first iteration ($t = 1$), the $x_k|_1^2$ is determined by the center of the optimization range; that is,

$$x_k|_1^2 = \frac{max - min}{2}, \tag{1}$$

**TABLE 1.** OA(18, 7, 3, 2) with three-level entries 1, 2, and 3.

| | | | | | | |
|---|---|---|---|---|---|---|
| 1 | 1 | 1 | 2 | 3 | 1 | 1 |
| 1 | 2 | 2 | 3 | 2 | 2 | 3 |
| 1 | 3 | 3 | 1 | 1 | 3 | 2 |
| 2 | 1 | 2 | 1 | 2 | 3 | 1 |
| 2 | 2 | 3 | 2 | 1 | 1 | 3 |
| 2 | 3 | 1 | 3 | 3 | 2 | 2 |
| 3 | 1 | 3 | 3 | 2 | 1 | 2 |
| 3 | 2 | 1 | 1 | 1 | 2 | 1 |
| 3 | 3 | 2 | 2 | 3 | 3 | 3 |
| 1 | 1 | 3 | 1 | 3 | 2 | 3 |
| 1 | 2 | 1 | 2 | 2 | 3 | 2 |
| 1 | 3 | 2 | 3 | 1 | 1 | 1 |
| 2 | 1 | 1 | 3 | 1 | 3 | 3 |
| 2 | 2 | 2 | 1 | 3 | 1 | 2 |
| 2 | 3 | 3 | 2 | 2 | 2 | 1 |
| 3 | 1 | 2 | 2 | 1 | 2 | 2 |
| 3 | 2 | 3 | 3 | 3 | 3 | 1 |
| 3 | 3 | 1 | 1 | 2 | 1 | 3 |

where, *min* and *max* are the lower bound and upper bound of the optimization range for a parameter, respectively. The other two level values can be obtained by

$$x_k|_1^1 = x_k|_1^2 - LD_1, \tag{2}$$
$$x_k|_1^3 = x_k|_1^2 + LD_1, \tag{3}$$

and the level difference $LD_1$ ($t = 1$) is

$$LD_1 = \frac{max - min}{\text{number of level} + 1}. \tag{4}$$

By using the OA(18, 7, 3, 2), 18 experiments, which are EM simulations in this study, are conducted according to a set of seven optimization parameters. The fitness value of each experiment is evaluated using a fitness function, which is relative to the optimization goal. After that, the fitness value of the $n$-th experiment is converted to a corresponding signal-to-noise (S/N) ratio, $\eta$, using (5),

$$\eta = -20\log(Fitness). \tag{5}$$

Apparently, a smaller fitness value results in a larger $\eta$. After conducting all 18 experiments, a response table shown in Table 2 is built based on the S/N ratios obtained by (5). The entries in the response table are the mean S/N ratios $\bar{\eta}(s,\ k)$ of each level $s$ and each parameter $k$ in OA($n$, $k$) = $s$; that is,

$$\bar{\eta}(s,\ k) = \frac{1}{6}\sum_{\text{OA}(n,k)=s} \eta_n;\ n = 1 \text{ to } 18. \tag{6}$$

Next, finding the largest $\bar{\eta}$ in each column of the response table can identify the optimal level value for that parameter. Once the optimal level value of each parameter is identified, a confirmation experiment will be performed at the end of the

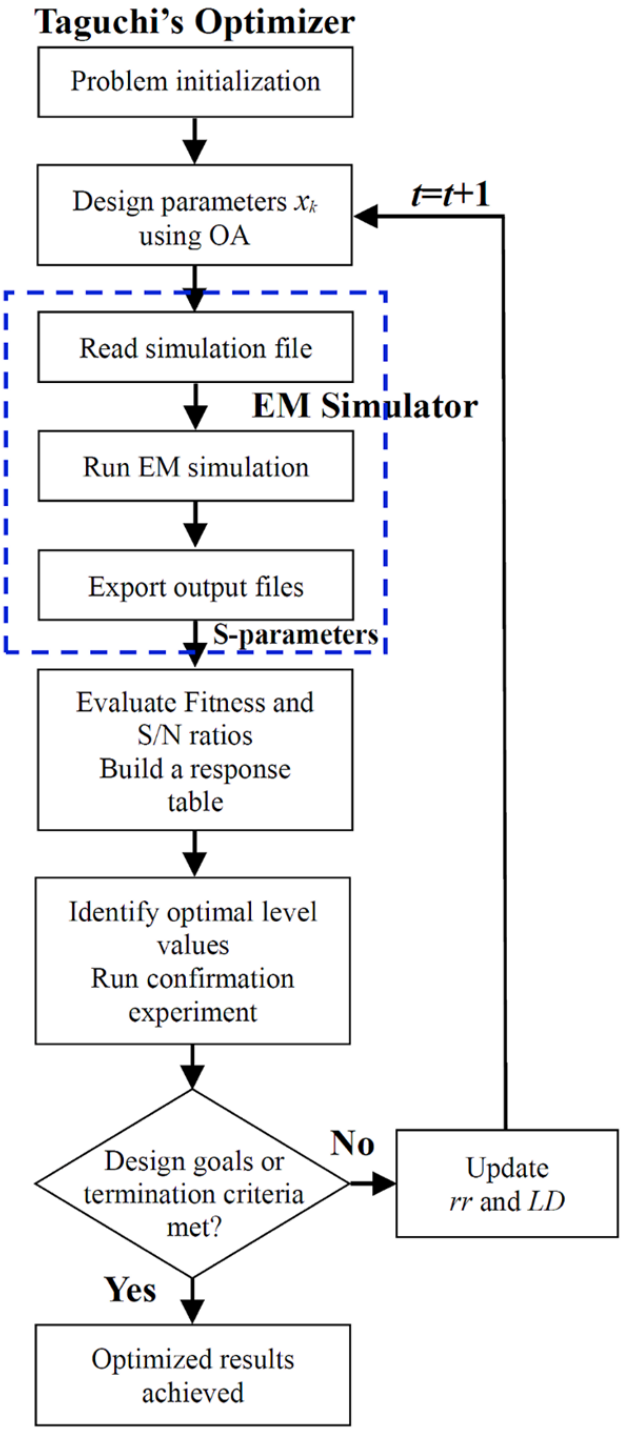


**FIGURE 3.** Flow diagram of Taguchi's method in conjunction with a full-wave EM simulator.

current iteration using the combination of the optimal level values because this combination may not be included in the OA. Its fitness will also be examined for optimization. The optimization process will end if the optimal result, which is usually measured by the best fitness value, meets the design goal or the termination criteria is reached; otherwise, the iterative optimization process will continue. Consequently,

**TABLE 2.** Response table.

| Level \ Par. | 1 | 2 | 3 | 4 | 5 | 6 | 7 |
|---|---|---|---|---|---|---|---|
| 1 | $\bar{\eta}(1,2)$ | $\bar{\eta}(1,2)$ | $\bar{\eta}(1,3)$ | $\bar{\eta}(1,4)$ | $\bar{\eta}(1,5)$ | $\bar{\eta}(1,6)$ | $\bar{\eta}(1,7)$ |
| 2 | $\bar{\eta}(2,2)$ | $\bar{\eta}(2,2)$ | $\bar{\eta}(2,3)$ | $\bar{\eta}(2,4)$ | $\bar{\eta}(2,5)$ | $\bar{\eta}(2,6)$ | $\bar{\eta}(2,7)$ |
| 3 | $\bar{\eta}(3,1)$ | $\bar{\eta}(3,2)$ | $\bar{\eta}(3,3)$ | $\bar{\eta}(3,4)$ | $\bar{\eta}(3,5)$ | $\bar{\eta}(3,6)$ | $\bar{\eta}(3,7)$ |

the center level value $x_k|_{t+1}^{2}$ and the level difference $LD_{t+1}$ between the other two level values for the next $((t+1)$-th) iteration will be proceeded. If a three-level OA is used, the center level value $x_k|_{t+1}^{2}$ for the next iteration can simply be assigned by the current optimal level value $x_k|_{t}^{opt}$, that is,

$$x_k|_{t+1}^{2} = x_k|_{t}^{opt} \ , \tag{7}$$

The $LD_{t+1}$ for the next iteration can be determined by (8),

$$LD_{t+1} = rr\, LD_t \ , \tag{8}$$

where, $rr$ is the reduced rate to reduce the optimization range of each parameter for a converged result. The other two level values for the next iteration are determined by (9a) and (9b),

$$x_k|_{t+1}^{1} = x_k|_{t+1}^{2} - LD_{t+1} \ , \tag{9a}$$
$$x_k|_{t+1}^{3} = x_k|_{t+1}^{2} + LD_{t+1} \ . \tag{9b}$$

Sometimes an $x_k$ might exceed the solution space during the optimization. To deal with this situation, a boundary treatment used in this study is as follows. That is, if an $x_k$ is smaller than *min* or larger than *max*, the $x_k$ is simply set to be *min* or *max*, respectively.

If $x_k|_{t}^{opt} = min$ , the three level values for the next iteration are determined by (10a) to (10c) to ensure that the $x_k|_{t}^{opt}$ is included in one of the three levels and the other two level values are properly treated,

$$x_k|_{t+1}^{1} = min \ , \tag{10a}$$
$$x_k|_{t+1}^{2} = x_k|_{t+1}^{1} + LD_{t+1} \ , \tag{10b}$$
$$x_k|_{t+1}^{3} = x_k|_{t+1}^{1} + 2 \cdot LD_{t+1} \ . \tag{10c}$$

Using the similar manner, if $x_k|_{t}^{opt} = max$ , the three level values for the next iteration are determined by (10d) to (10f),

$$x_k|_{t+1}^{1} = max \ , \tag{10d}$$
$$x_k|_{t+1}^{2} = x_k|_{t+1}^{1} - LD_{t+1} \ , \tag{10e}$$
$$x_k|_{t+1}^{3} = x_k|_{t+1}^{1} - 2 \cdot LD_{t+1} \ . \tag{10f}$$

The following equation may be used as a termination criterion for the optimization procedure:

$$\frac{LD_{t+1}}{LD_1} \leq cv, \tag{11}$$

where, $cv$ is the converged value and it usually can be set between 0.001 and 0.01 depending on the problem. The

values of $rr = 0.9$ and $cv = 0.01$ are chosen in this BPF optimization.

For concise reasons, this study focuses only on the design and optimization of the proposed wideband BPF using the Taguchi's method, hence, other optimization techniques are not applied to the BPF; thus, optimization comparisons are not provided in this study, either. In addition, other detailed concepts and procedures of Taguchi's method are not described here and they can be found in [3] and [4].

### B. THE WIDEBAND BPF OPTIMIZATION

For the proposed wideband BPF optimization, the Taguchi's method determines the dimensions of the filter for IE3D while IE3D provides accurately simulated scattering parameters (S-parameters) for the fitness calculation. The optimization process does not require any manual adjustments. Furthermore, a fine mesh setting (25 cells/wavelength) in IE3D was used to obtain accurate EM simulation results while considering less time consumption for EM simulations.

According to the proposed wideband BPF design mechanism described in *Section II A*, an initial BPF is designed and its seven key parameters, $L_1$, $L_2$, $L_3$, $L_4$, $L_5$, $L_6$, and $w_2$, are chosen for Taguchi's optimization to achieve the desired wideband characteristics. The initial values and optimization ranges for each parameter are given in Table 3. Other dimensions shown in Fig. 2 are fixed at $w_1 = 0.2$ mm, $w_3 = 0.635$ mm, $a = 0.32$ mm, $g = 0.12$ mm, $w_{50} = 1.77$ mm, and $L_{50} = 3.5$ mm during optimization. It is worthwhile to note that the initial values are only used to create the initial BPF configuration in IE3D and set the optimization range for each parameter. It is not necessary to require the initial BPF to have good performance. The Taguchi's method will attempt to find the optimal solution in the given optimization range, as the proposed Taguchi's method is a global optimizer [3].

**TABLE 3. Initial values, optimization range, and optimized values of the BPF.**

(Unit: mm)

| Parameter | Initial value | Optimization range (*min-max*) | Optimized value |
|---|---|---|---|
| $L_1$ | 19.4 | 16.4-25.4 | 18.39 |
| $L_2$ | 2.5 | 1.5-4.5 | 4.45 |
| $L_3$ | 14.3 | 4.3-15.5 | 13.67 |
| $L_4$ | 1.0 | 0.4-2.0 | 1.51 |
| $L_5$ | 10.0 | 0-25.0 | 10.30 |
| $L_6$ | 3.4 | 1.9-5.4 | 1.99 |
| $w_2$ | 0.2 | 0.12-0.45 | 0.40 |

The optimization range, which is the difference between the lower bound and upper bound of a parameter, is greatly important for rapid convergence. It should be deliberately selected. Optimization range of a parameter is normally determined on the basis of the following guidelines:

1) in 50% and 200% variation of the initial value for the lower bound and upper bound, respectively.
2) no overlapping with other parameters.
3) no exceeding the substrate region.
4) manufacturing precision.

The optimization goals of the proposed BPF are divided into three frequency regions. They are defined as:

***Region I*:** $|S_{21}(f)| < S_{21}, d = -35$ dB, *for* $0.5 \le f \le 1.5$ GHz ,

***Region II*:** $|S_{11}(f)| < S_{11}, d = -20$ dB, *for* $1.7 \le f \le 3.2$ GHz ,

***Region III*:** $|S_{21}(f)| < S_{21}, d = -35$ dB, *for* $3.4 \le f \le 4.5$ GHz .

Where, $S_{11}, d$ and $S_{21}, d$ are the desired reflection coefficient and transmission coefficient magnitudes of the BPF, respectively. It is worthwhile to note that to ensure the measured S-parameters of the BPF to meet the design specifications, a treatment used here is to set the optimization goals more rigorously than the design specifications, which are described in *Section II B*. Hence, the fitness function for the Taguchi's optimization is described in (12):

$$Fitness = C1 \cdot fit1 + C2 \cdot fit2 + C3 \cdot fit3 \ , \quad (12)$$

where (13)–(15), as shown at the bottom of the next page, $fit1, fit2$, and $fit3$ calculate the fitness values in *Region I*, *Region II*, and *Region III,* respectively; $C1, C2$, and $C3$ are the corresponding weights in each region. $\Delta f$ is the frequency interval set to be 0.01 GHz. In (13) to (15), sgn [ ] equals 1 if the entry is positive whereas sgn [ ] equals -1 if the entry is negative. Equations (13) and (15) are used to obtain high rejection and selectivity in the stopband whereas (14) is applied to acquire good impedance match in the passband. The fitness value is a parameter relative to the BPF to be designed, such as the reflection coefficient and the transmission coefficient of the BPF. If $|S_{11}(f)|$ is higher than $S_{11}, d$ ($-20$ dB) in *Region II*, computing the fitness value is performed at frequencies between 1.7 and 3.2 GHz. However, computing the fitness value is not performed when $|S_{11}(f)|$ is less than $S_{11}, d$. The same process is also applied to the fitness value calculations on the transmission coefficient $|S_{21}(f)|$ in *Region I* and *Region III*. In the optimization settings, the weights are chosen as follows: $C1$=10, $C2$=1, and $C3$=10. $C1$ and $C3$ are set larger than $C2$ because the differences between $|S_{21}(f)|$ and $S_{21}, d$ in *Region I* and *Region III* are emphasized to obtain high rejection and selectivity in the stopband. The fitness value of (12) represents the difference between the S-parameters and the desired limits on the decibel scale to evaluate the performance of the current EM simulated results. Clearly, a smaller fitness value reflects a better BPF performance.

For the optimized method, the proposed filter is optimized with a large number of parameters and a wide optimization

range of each parameter. Therefore, the proposed filter optimization can be considered a challenging design.

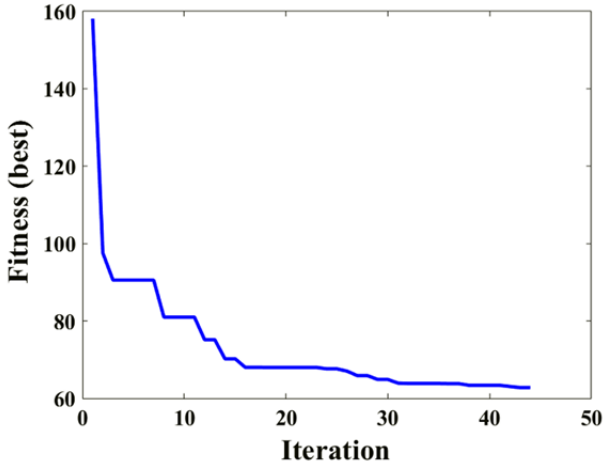


**FIGURE 4.** The fitness curve of the wideband BPF optimization.

## IV. RESULTS AND DISCUSSIONS

The wideband BPF optimization was performed on a personal computer with a 2.9 GHz Intel i7 870 CPU and 8 GB of memory. After 44 iterations (total $19 \times 44 = 836$ EM simulations), the optimization process was ended since the termination criterion shown in (11) was met. Fig. 4 reveals the fitness curve of the BPF optimization. The fitness values are significantly reduced in the first 20 iterations, showing a great optimization ability of the Taguchi's method. Then the fitness values converge to the end of iteration. The dimensions of the optimized BPF are also listed in Table 3. Later, the optimized BPF is fabricated on a *Rogers* RO 4003C substrate and tested by an Agilent 5230A vector network analyzer. The photograph of the optimized BPF fabricated on the substrate is illustrated in Fig. 5. The optimized BPF has a compact size (with clearance) less than 18.8 mm by 21.3 mm, which corresponds to 0.25 $\lambda$g by 0.28 $\lambda$g, where $\lambda$g (75.3 mm) is the guided wavelength at the center frequency ($f_0$) of 2.4 GHz. Simulated and measured S-parameters of the optimized BPF are plotted together in Fig. 6 for comparisons. Apparently, good agreements between simulated and measured S-parameters are observed. This validates the proposed filter design. The measured return loss (RL) is greater than 15 dB within the passband showing good impedance match. Furthermore, for the measured insertion loss (IL), rejection levels of more than 42 dB at the lower stopband in *Region I* and better than 31 dB at the higher stopband in *Region III* are achieved. Meanwhile, the filtering features of high selectivity and steep skirt in the stopbands are also revealed.

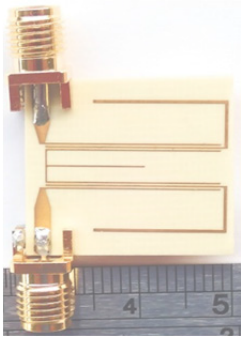

**FIGURE 5.** The photograph of the optimized BPF.

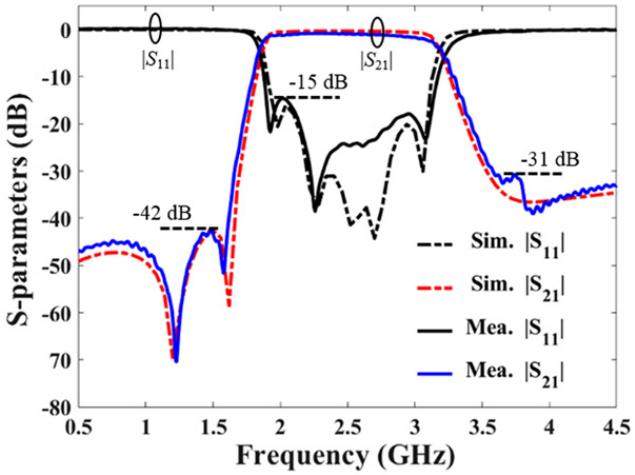


**FIGURE 6.** S-parameters of the proposed wideband BPF.

Fig. 7 exhibits the enlargement of the transmission coefficients in the passband. The BPF has a wide 3 dB FBW of 55.2% (1.85 GHz - 3.19 GHz) for the measured IL, where its minimum value is 0.43 dB at 2.18 GHz.

Fig. 8 shows the group delays of the proposed wideband BPF. Reasonable agreements between simulated and

$$fit1 = \sum_{f=0.5\,\mathrm{GHz}}^{1.5\,\mathrm{GHz}} [(|S_{21}(f)| - S_{21}, d)]\{\frac{1 + \mathrm{sgn}[|S_{21}(f)| - S_{21}, d]}{2}\}\Delta f, \tag{13}$$

$$fit2 = \sum_{f=1.7\,\mathrm{GHz}}^{3.2\,\mathrm{GHz}} [(|S_{11}(f)| - S_{11}, d)]\{\frac{1 + \mathrm{sgn}[|S_{11}(f)| - S_{11}, d]}{2}\}\Delta f, \tag{14}$$

$$fit3 = \sum_{f=3.4\,\mathrm{GHz}}^{4.5\,\mathrm{GHz}} [(|S_{21}(f)| - S_{21}, d)]\{\frac{1 + \mathrm{sgn}[|S_{21}(f)| - S_{21}, d]}{2}\}\Delta f. \tag{15}$$

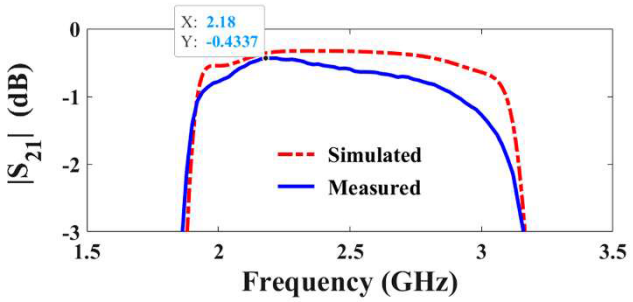


**FIGURE 7.** The enlargement of transmission coefficients in the passband.

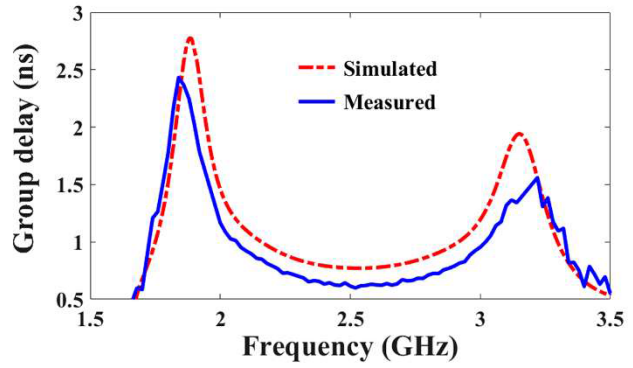


**FIGURE 8.** Group delays of the proposed wideband BPF in the passband.

measured group delays are also observed. The measured group delay is about 0.6 ns at the center frequency. Variations in the measured group delays are small, and flat group delays are revealed in the central region of the passband. These results show that signals with a good linear-phase response can be ensured on the proposed wideband BPF. Hence, the proposed wideband BPF can be used for high-capacity communication systems [1].

**TABLE 4.** Comparison with other recently reported wideband BPFs.

| BPFs | $\varepsilon_r$ / $h$ (mm) | $f_0$ (GHz) / FBW (%) | Min. IL / RL (dB) | Size ( $\lambda g^2$ at $f_0$ ) |
|---|---|---|---|---|
| [15] | 2.65/1.0 | 2.1/19.0 | 1.8/12 | 0.28 × 0.39 |
| [16] | 2.2/0.787 | 3.5/9.0 | 1.03/14 | 0.42 × 0.8 |
| [17] | 3.55/0.813 | 2.0/40.0 | 1.0/15 | N/A |
| [18] | 3.55/0.813 | 2.5/50.0 | 0.5/16 | 0.48 × 1.5 |
| **This work** | 3.55/0.813 | 2.4/**55.2** | **0.43/15** | **0.25 × 0.28** |

Table 4 tabulates the performance comparisons of the proposed BPF with other state-of-the-art microstrip wideband BPFs, which were recently reported in [15], [16], [17], and [18]. The comparisons show that the proposed wideband BPF demonstrates better performance in the passband characteristics, FBW, IL, and size.

In summary, Taguchi's method successfully achieves the design specifications of the proposed wideband BPF. The results demonstrate that the proposed BPF performs well. The proposed BPF is highly suitable for 2.4 GHz WLAN systems.

## V. CONCLUSION

A compact microstrip bandpass filter with wideband, high selectivity, steep skirt, and flat frequency characteristics has been designed and optimized by the Taguchi's method. The BPF design mechanism and the concepts of the Taguchi's method have been given. Moreover, guidelines for the determination of the parameter optimization range for rapid convergence have also been provided. Using the Taguchi's method integrated with the full-wave EM simulator, the design and optimization of the wideband BPF can quickly be implemented. The measured 3 dB FBW of the optimized BPF is found to be 55.2%. The simulated results have evidently been found in good agreement with the measured ones, confirming the validity of the proposed method. The proposed BPF has shown excellent performance compared with other microstrip wideband BPFs. Consequently, the proposed optimization approach is promising for designing novel microstrip filters.

## REFERENCES

[1] J. S. Hong and M. J. Lancaster, *Microstrip Filters for RF/Microwave Applications*, 2nd ed. New York, NY, USA: Wiley, 2001, pp. 62–68.
[2] G. Taguchi, S. Chowdhury, and Y. Wu, *Taguchi's Quality Engineering Handbook*. New York, NY, USA: Wiley, 2005, ch. 4.
[3] W. C. Weng, F. Yang, and A. Z. Elsherbeni, "Linear antenna array synthesis using Taguchi's method: A novel optimization technique in electromagnetics," *IEEE Trans. Antennas Propag.*, vol. 55, no. 3, pp. 723–730, Mar. 2007, doi: 10.1109/TAP.2007.891548.
[4] W. C. Weng, F. Yang, and A. Z. Elsherbeni, *Electromagnetics and Antenna Optimization Using Taguchi's Method*. San Rafael, CA, USA: Morgan & Claypool, 2007, pp. 1–84.
[5] W. C. Weng and C. T. M. Choi, "Optimal design of CPW slot antennas using Taguchi's method," *IEEE Trans. Magn.*, vol. 45, no. 3, pp. 1542–1545, Mar. 2009, doi: 10.1109/TMAG.2009.2012737.
[6] J.-H. Ko, J.-K. Byun, J.-S. Park, and H.-S. Kim, "Robust design of dual band/polarization patch antenna using sensitivity analysis and Taguchi's method," *IEEE Trans. Magn.*, vol. 47, no. 5, pp. 1258–1261, May 2011, doi: 10.1109/TMAG.2010.2081663.
[7] X. Jia and G. Lu, "An improved random Taguchi's method based on swarm intelligence and dynamic reduced rate for electromagnetic optimization," *IEEE Antennas Wireless Propag. Lett.*, vol. 18, no. 9, pp. 1878–1881, Sep. 2019, doi: 10.1109/LAWP.2019.2932088.
[8] S. E. Nai, Z. Lei, S. H. Wong, and Y. H. Chew, "Optimizing radio network parameters for vertical sectorization via Taguchi's method," *IEEE Trans. Veh. Technol.*, vol. 65, no. 2, pp. 860–869, Feb. 2016, doi: 10.1109/TVT.2015.2401030.
[9] A. Awada, B. Wegmann, I. Viering, and A. Klein, "Optimizing the radio network parameters of the long term evolution system using Taguchi's method," *IEEE Trans. Veh. Technol.*, vol. 60, no. 8, pp. 3825–3839, Oct. 2011, doi: 10.1109/TVT.2011.2163326.
[10] M. A. Zaman and M. A. Matin, "Optimization of Jiles-Atherton hysteresis model parameters using Taguchi's method," *IEEE Trans. Magn.*, vol. 51, no. 5, pp. 1–4, May 2015.

[11] *IE3D User's Manual, Release 11*, Zeland Software, Inc., Fremont, CA, USA, Feb. 2005.

[12] L. Li and Z.-F. Li, "Side-coupled shorted microstrip line for compact quasi-elliptic wideband bandpass filter design," *IEEE Microw. Wireless Compon. Lett.*, vol. 20, no. 6, pp. 322–324, Jun. 2010, doi: 10.1109/LMWC.2010.2047516.

[13] F. Huang, J. Wang, J. Li, and W. Wu, "Compact microstrip wideband bandpass filter with high selectivity," *Electron. Lett.*, vol. 52, no. 8, pp. 626–628, Apr. 2016, doi: 10.1049/EL.2015.4539.

[14] N. J. A. Sloane. *A Library of Orthogonal Arrays*. Accessed: Aug. 15, 2022. [Online]. Available: http://neilsloane.com/oadir/

[15] K. D. Xu, F. Zhang, Y. Liu, and Q. H. Liu, "Bandpass filter using three pairs of coupled lines with multiple transmission zeros," *IEEE Microw. Wireless Compon. Lett.*, vol. 28, no. 7, pp. 576–578, Jul. 2018, doi: 10.1109/LMWC.2018.2835643.

[16] G. Chaudhary and Y. Jeong, "Arbitrary prescribed flat wideband group delay absorptive microstrip bandpass filters," *IEEE Trans. Microw. Theory Techn.*, vol. 69, no. 2, pp. 1404–1414, Feb. 2021, doi: 10.1109/TMTT.2020.3041483.

[17] R. Zhang, S. Luo, and L. Zhu, "A new synthesis and design method for wideband bandpass filters with generalized unit elements," *IEEE Trans. Microw. Theory Techn.*, vol. 65, no. 3, pp. 815–823, Mar. 2017, doi: 10.1109/TMTT.2016.2636825.

[18] M. Á. Sánchez-Soriano and C. Quendo, "Systematic design of wideband bandpass filters based on short-circuited stubs and λ/2 transmission lines," *IEEE Microw. Wireless Compon. Lett.*, vol. 31, no. 7, pp. 552–849, Jul. 2021, doi: 10.1109/LMWC.2021.3076924.

**WEI-CHUNG WENG** (Senior Member, IEEE) received the B.S. degree in electronic engineering from the National Changhua University of Education, Changhua, Taiwan, in 1993, the M.S. degree in electrical engineering from I-Shou University, Kaohsiung, Taiwan, in 2001, and the Ph.D. degree in electrical engineering from the University of Mississippi, MS, USA, in 2007.

From 2004 to 2007, he was a Graduate Research Assistant at the Department of Electrical Engineering, University of Mississippi. In 2008, he joined at the Department of Electrical Engineering, National Chi Nan University, Puli, Taiwan, where he is currently an Associate Professor. From 2017 to 2018, he was a Visiting Scholar at the Department of Electrical Engineering, Colorado School of Mines, Golden, CO, USA. He coauthored a book titled *Electromagnetics and Antenna Optimization Using Taguchi Method* (Morgan & Claypool, 2007). His research interests include antenna and microwave circuit design, computational electromagnetics, electromagnetic compatibility, and optimization techniques in electromagnetics.

Dr. Weng is a member of ACES and a Life Member of the Institute of Antenna Engineers of Taiwan (IAET). He was the recipient of the Outstanding Teaching Award, in 2013, 2016, and 2019, and the Teaching Contribution Award, in 2020, from National Chi Nan University. He is currently the Associate Editor-in-Chief of *Applied Computational Electromagnetics Society (ACES) Journal*.